AGU100 ADVANCING EARTH AND SPACE SCIENCE

Water Resources Research

RESEARCH ARTICLE
10.1029/2019WR025003

Key Points:
- Film flow held by adsorption forces is thought to be the dominant process for supporting the fast falling evaporation rate stage
- A theoretical model that accounts for film flow was developed for evaporation rate estimation
- The proposed model, requiring no adjustable parameters, yields close agreement with both laboratory and field observations

A Physically Based Method for Soil Evaporation Estimation by Revisiting the Soil Drying Process

Yunquan Wang[1,2], Olivier Merlin[3], Gaofeng Zhu[4], and Kun Zhang[5]

[1]School of Environmental Studies, China University of Geosciences, Wuhan, China, [2]Laboratory of Basin Hydrology and Wetland Eco-restoration, China University of Geosciences, Wuhan, China, [3]CESBIO, Université de Toulouse, CNES-CNRS-IRD-UPS, Toulouse, France, [4]Key Laboratory of Western China's Environmental Systems (Ministry of Education), Lanzhou University, Lanzhou, China, [5]Institute of Tibetan Plateau Research, Chinese Academy of Sciences, Beijing, China

Abstract While numerous models exist for soil evaporation estimation, they are more or less empirically based either in the model structure or in the determination of introduced parameters. The main difficulty lies in representing the water stress factor, which is usually thought to be limited by capillarity-supported water supply or by vapor diffusion flux. Recent progress in understanding soil hydraulic properties, however, have found that the film flow, which is often neglected, is the dominant process under low moisture conditions. By including the impact of film flow, a reexamination on the typical evaporation process found that this usually neglected film flow might be the dominant process for supporting the Stage II evaporation (i.e., the fast falling rate stage), besides the generally accepted capillary flow-supported Stage I evaporation and the vapor diffusion-controlled Stage III evaporation. A physically based model for estimating the evaporation rate was then developed by parameterizing the Buckingham-Darcy's law. Interestingly, the empirical Bucket model was found to be a specific form of the proposed model. The proposed model requires the in-equilibrium relative humidity as the sole input for representing water stress and introduces no adjustable parameter in relation to soil texture. The impact of vapor diffusion was also discussed. Model testing with laboratory data yielded an excellent agreement with observations for both thin soil and thick soil column evaporation experiments. Model evaluation at 15 field sites generally showed a close agreement with observations, with a great improvement in the lower range of evaporation rates in comparison with the widely applied Priestley and Taylor Jet Propulsion Laboratory model.

Correspondence to:
Y. Wang,
wangyq@cug.edu.cn

Citation:
Wang, Y., Merlin, O., Zhu, G., & Zhang, K. (2019). A physically based method for soil evaporation estimation by revisiting the soil drying process. *Water Resources Research*, *55*, 9092–9110. https://doi.org/10.1029/2019WR025003

Received 16 FEB 2019
Accepted 11 OCT 2019
Accepted article online 24 OCT 2019
Published online 14 NOV 2019

1. Introduction

Soil evaporation plays an important role in the mass and energy exchange between the land surface and the atmosphere. Together with plant transpiration, they return about 60% of precipitation into the air (Oki & Kanae, 2006) and consume nearly 25% of the incoming solar radiation globally (Trenberth et al., 2009). Estimating soil evaporation accurately and separating its contribution from the plant transpiration are crucial to understand the water and energy cycles (Gu et al., 2018; Maxwell & Condon, 2016; Seneviratne et al., 2010; Wang & Dickinson, 2012) and to quantify the carbon cycle process that is highly related to plant behavior (Fisher et al., 2017; Schlesinger & Jasechko, 2014; Sutanto et al., 2012). Physically, soil evaporation is the transition of soil water from the liquid phase to the vapor phase and the escape of water vapor to the above atmosphere. The phase transition requires an energy supply while the vapor escape is mainly a molecule diffusion process (Haghighi et al., 2013). By focusing mainly on energy supply or on vapor transport process, the existing evaporation estimation methods can generally be summarized into two series: the energy budget one and the mass transfer one (Brutsaert, 2005).

The energy budget methods vary in different forms, among them, the classic one relies on the concepts of atmospheric demand and water supply. The atmospheric demand is represented by the potential evaporation rate, often estimated by the Penman (1948) equation or by the Priestley and Taylor (1972) equation. The water supply, also known as the water stress factor, is usually expressed empirically as a linear function of soil water content after the identification of a "critical water content" below, which soil water supply is limited (Seneviratne et al., 2010). This kind of method, also termed as the Bucket model (Brutsaert, 2005;

Budyko, 1974), is probably the oldest method of evaporation estimation. Due to its simplicity (which may vary in different forms), it is still extensively applied, in particular within remote sensing-based evaporation models (e.g., Fisher et al., 2008; Martens et al., 2017; Miralles et al., 2011).

The mass transfer- or resistance-based methods consider the vapor transfer process in a direct way. The evaporation process is described as vapor diffusion from either the soil surface or a depth below. The former is the so-called α formulation (e.g., Barton, 1979; Noilhan & Planton, 1989). An aerodynamic resistance term is introduced to represent the vapor transfer efficiency from soil surface to the atmosphere. When the evaporation process is considered from a plane below the soil surface, where vapor pressure is saturated, an additional soil surface resistance term is included, leading to the so-called β formulation (e.g., Deardorff, 1977; Dorman & Sellers, 1989).

The Bucket model and the resistance-based methods, although widely applied, are somehow empirically based, especially in determining the water stress and the resistance factors. The linear relationship in the Bucket model is empirical (Brutsaert, 2005; Seneviratne et al., 2010) and might not be unique even in the same location (Haghighi et al., 2018). The resistance methods, although physically based, rely on empirical estimation of the resistance terms (e.g., Mahfouf & Noilhan, 1991; Merlin et al., 2016, 2018). The ambiguities in parameter estimation methods, as well as the difficulty in accurate data acquisition (e.g., the surface water content and the soil hydraulic properties), therefore, would introduce high uncertainty in evaporation rate estimation.

Alternatively, the soil evaporation can be estimated from the perspective of soil water transport ability. Instead of being represented as a stress factor or a resistance term (usually expressed empirically) as in the former methods, the soil water supply can be calculated directly, and the actual evaporation rate is regarded as the minimum term between the soil water flux and the potential evaporation rate. This method is termed as the threshold formulation (e.g., Dickinson, 1984; Mahrt & Pan, 1984). With the soil water flux described physically by the Buckingham-Darcy's law, which can be calculated by solving the Richards equation (e.g., Sutanto et al., 2012) or by parameterizing over a thin soil surface layer (e.g., Mahrt & Pan, 1984), this method provides a much more solid basis for evaporation estimation. In the literature, for a drying process, capillary flow is regarded as the main soil water flow form, and vapor diffusion is included when soil becomes very dry (Lehmann et al., 2008; Or et al., 2013; Or & Lehmann, 2019; Philip & de Vries, 1957; Saito et al., 2006).

However, such capillary flow- and vapor diffusion-supported evaporation process may be problematic for not considering the potential impact of film flow. This thin film-form water, held by the adsorption forces on the soil particle surface, is usually treated as unremovable and, hence, be unimportant in water flow process (e.g., Idso et al., 1974; Philip & de Vries, 1957). Recent progress in soil hydraulic properties modeling, however, has found that this film flow is in fact the predominant water flow form under low moisture conditions (e.g., Tuller & Or, 2001; Wang et al., 2013, 2018). By including this film flow, the newly proposed soil hydraulic models greatly improved the performance under low moisture conditions in comparison with capillary-based models (Lebeau & Konrad, 2010; Peters, 2013; Tuller & Or, 2001; Wang et al., 2016, 2017, 2018). The re-recognition of the importance of this thin film, therefore, requires us to reconsider the soil evaporation process, which is commonly assumed to be supported only by capillary flow and vapor diffusion. Although early research in the engineering area has taken into account the impact of the so-called bound water (e.g., Chen & Pei, 1989), the analysis was problematic due to the unclear definition of the hydraulic conductivity properties in relation to the bound water.

Hence, there are three main objectives in this study: 1) to reexamine the typical evaporation process by including the impact of film flow, besides the commonly recognized capillary flow and vapor diffusion; 2) to develop a theoretical evaporation estimation model based on the detailed analysis of the soil drying process; and 3) to evaluate the model performance with both laboratory and field observations.

2. Theoretical Development

2.1. The Soil Drying Process Revisited

As shown in Figure 1a, the typical evaporation process from an initially saturated soil column can be generally distinguished into the energy-limited stage and the moisture-limited stage, respectively (e.g.,

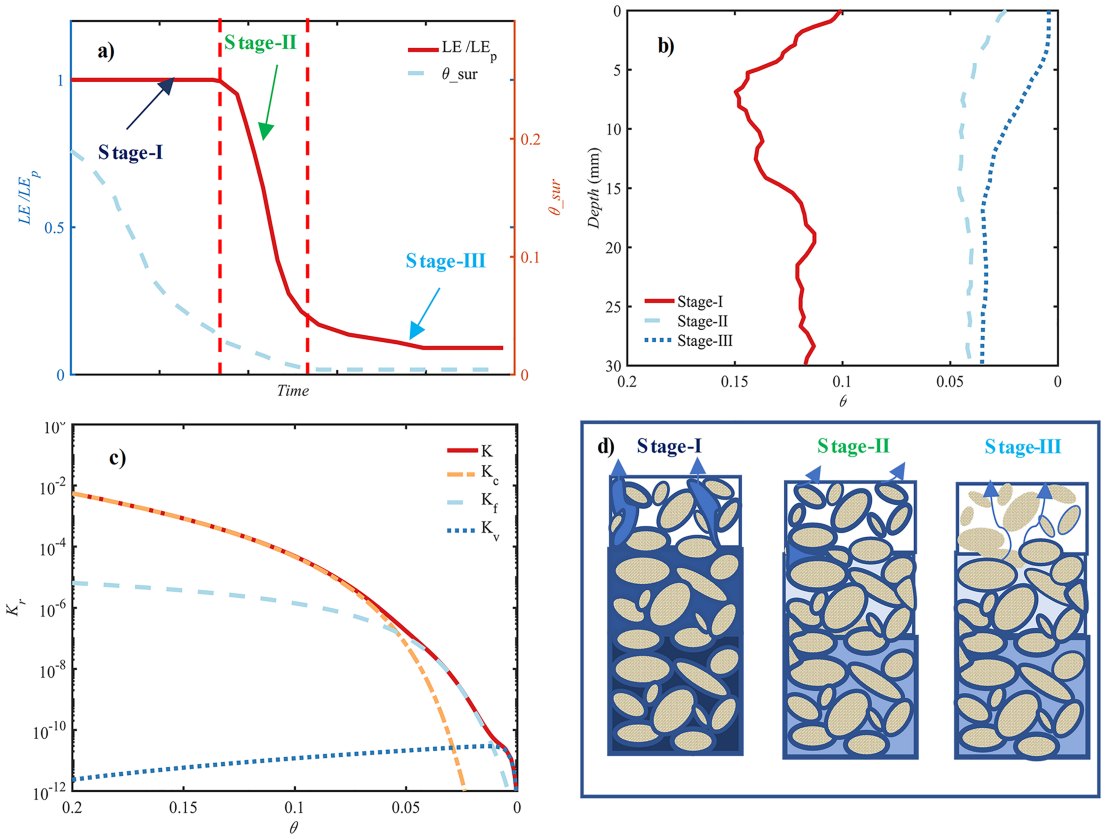

Figure 1. (a) Illustration of the normalized evaporation rate and the predicted soil surface water content from an initial saturated soil column. Three stages are identified, including the near constant rate Stage I evaporation, the fast falling rate Stage II evaporation, and the smoothly changing Stage III evaporation. (b) The near surface soil water content profiles observed by magnetic resonance imaging at different evaporation stages after Merz et al. (2015). (c) Illustration of the soil hydraulic conductivity curve over the complete moisture range with the Extention and Modification of the Fredlund and Xing (1994) model (termed as the EMFX model) proposed in Wang et al. (2016, 2017), including capillary flow (K_c), film flow (K_f), and vapor diffusion (K_v). The vapor diffusion is calculated following Saito et al. (2006). (d) Illustration of the typical soil water flow process under three stages, the soil particle is in yellow and the water is in blue. The Stage I evaporation is supported by capillary flow retained in soil pores, and the drying process is accompanied by an increase in the drying front depth. During Stage II evaporation, capillary flow can no longer reach soil surface directly, and the drying process is limited by film flow along soil particle surface dominated in a thin—several millimeters in depth—soil surface layer. Under Stage III evaporation, this thin soil surface layer is almost completely dried (with water content be equal to the air-dry water content), and vapor diffusion becomes the dominant process in this layer.

Lehmann et al., 2008; Or et al., 2013; Shokri & Or, 2011). The energy-limited stage is also termed as Stage I evaporation. When the atmospheric demand keeps constant, this stage would have a constant evaporation rate (assuming the impact of capillary limitations and nonlinear boundary layer interactions are not important), so it is also known as the constant-rate period (e.g., Yiotis et al., 2007). The moisture-limited stage can be subdivided into two stages: the Stage II or the transition stage marked by a fast falling evaporation rate and the Stage III where evaporation rate keeps low and changes smoothly (e.g., Idso et al., 1974; Merz et al., 2015).

Correspondingly, the soil water flow supporting the drying process can also be divided into three forms, including the commonly recognized capillary flow in full pores and in corners and the vapor diffusion in void pores, as well as the usually neglected thin film flow on soil particle surfaces (Peters, 2013; Tuller & Or, 2001; Wang et al., 2018). Notably, this thin film flow held by adsorption forces is different from the so-called "thick film flow" presented in the literature (e.g., Lehmann et al., 2008; Yiotis et al., 2003, 2007, 2012), where it represents the water flow supported mostly by capillarity and controls the water transport between the saturated zone and the evaporation surface. In these referred work, this thin film flow was assumed to be unimportant and then be neglected (Yiotis et al., 2007).

2.1.1. The Stage I Evaporation

For the drying process, the Stage I evaporation is extensively studied (e.g., Lehmann et al., 2008, 2018; Or et al., 2013; Shahraeeni et al., 2012; Shokri et al., 2008 and references therein). In this period, an

efficient water supply between the drying front and the soil surface is maintained by capillary flow. The drying process is accompanied by a decrease in soil surface moisture and an increase in drying front depth. The end of this period should depend on both the capillary flow ability and the atmospheric demand. However, because the capillarity-supported water supply is usually higher than the atmospheric demand even under low water saturation conditions (Shahraeeni et al., 2012), the Stage I evaporation generally ends when a critical surface water content or a characteristic depth is reached, where the capillary water potential gradient between the drying front and the soil surface cannot overcome the gravitational forces and viscous dissipation (Lehmann et al., 2008). This critical water content then can be seen as air begins to invade the finest pores at soil surface, and it is roughly corresponding to the so-called residual water content (Or et al., 2013). The duration of the Stage I evaporation is therefore determined by soil pore size distribution properties. In this period, the evaporation rate is generally equal to the potential evaporation rate. However, it should be noted that for very fine textured soil and for high atmospheric demand, a higher critical water content and a lower evaporation rate are expected due to the resistance induced by viscous effects (Haghighi et al., 2013; Lehmann et al., 2018; Or & Lehmann, 2019) and/or due to the vapor exchange limitations across the air boundary layer (Haghighi & Or, 2013; Shahraeeni et al., 2012). In the present study, these effects are not included.

2.1.2. The Stage II Evaporation

While extensive research on Stage I evaporation exists in the literature, little work has been done on the Stage II evaporation (Shokri & Or, 2011). In the classic soil evaporation theory, when the capillary flow is interrupted at the end of Stage I evaporation, the vaporization plane begins to recede into the inside soil, and the vapor diffusion becomes dominant at the soil surface (Lehmann et al., 2008; Or et al., 2013; Philip & de Vries, 1957; Saito et al., 2006). Notably at this point, liquid water still exists at soil surface, mainly in the form of thin film adsorbed by soil particle (Tuller & Or, 2001; Wang et al., 2018). In the capillarity-based theory (e.g., Corey & Brooks, 1999; van Genuchten, 1980), this left liquid water is represented by the so-called residual water content and means the low limitation of the free water. Accordingly, it has nearly no contribution to the evaporation process.

This left and unremovable soil surface water content, however, is inconsistent with recent laboratory observations. For example, the magnetic resonance imaging of a sand column presented by Merz et al. (2015) demonstrated clearly a gradual decreasing soil surface moisture during the Stage II evaporation (see also Figure 1b). The vapor diffusion-dominated assumption is also inconsistent with laboratory observations. According to Fick's law, a vapor diffusion-controlled Stage II evaporation requires a gradually increased diffusion layer thickness to explain the fast-falling evaporation rate (Shokri et al., 2009; Shokri & Or, 2011). The dye experiment by Shokri and Or (2011), however, observed an abrupt jump of the vaporization plane at the end of the Stage II evaporation (the so-called transition period in Shokri & Or, 2011). This abrupt jump indicated that the vaporization plane should remain in the soil surface during the Stage II evaporation. In other words, the water transport near the soil surface is still dominated by liquid flow; otherwise, a gradually receding vaporization plane would be observed.

The gradually decreased soil surface moisture and the dominant liquid flow observed in Stage II evaporation happen to be consistent with recent progress in soil hydraulic properties modeling. Commonly used soil hydraulic models conceptualize pore space as a bundle of cylindrical capillaries (e.g., Mualem, 1976; van Genuchten, 1980), neglecting the flow in liquid films held by adsorption forces. This kind of capillary models often underestimate the hydraulic conductivities under dry conditions (e.g., Tuller & Or, 2001; Wang et al., 2013, 2018). Recently, a lot of research confirms that the liquid film, also explained as in corresponding to the residual water content in capillary-based model (Corey & Brooks, 1999), is actually flowable (Peters, 2013; Tokunaga, 2009; Tuller & Or, 2001; Wang et al., 2013). By including both capillary flow and film flow, recently proposed models significantly improve the model performance under dry conditions (Lebeau & Konrad, 2010; Peters, 2013; Tuller et al., 1999; Tuller & Or, 2001; Wang et al., 2016, 2017, 2018). An illustration in Figure 1c shows clearly that this neglected film conductivity is dominating after the soil moisture reaches the so-called residual water content while the vapor diffusion is only important under extremely dry conditions.

At pore scale, when air invades the finest pore at soil surface—marking the end of Stage I evaporation—liquid flow still exists in film form held by the adsorption force as well as in corner form retained by

capillarity. This is consistent with the following statement made by Scherer (1990) for the fast-falling rate evaporation period: "*The liquid in the pores near the surface remains in the funicular condition, so there are contiguous pathways along which flow can occur*" (see figure 4 in Scherer, 1990). Tuller and Or (2001) showed that the hydraulic conductivity resulting from corner flow was generally negligible in comparison with film flow under dry conditions. Therefore, the usually neglected film flow, rather than vapor diffusion, might be the supporting mechanism that limits the water supply during Stage II evaporation. The vapor diffusion also contributes to the evaporation process, however, in a magnitude generally less than liquid film flow.

Notably, this film dominant zone is restricted in a depth of several millimeters, below which, water flow is still supported by capillarity. During this stage, the evaporation process is also accompanied by a decrease in soil surface moisture while the drying front depth keeps almost constant due to the discontinuity of capillary flow (Lehmann et al., 2008;). Because the film flow flux is controlled by the soil specific surface area and the film thickness that depends on matric potential (Bird et al., 1960; Tokunaga, 2009), when considering film flow limitations solely, the soils with finer texture should generally have a higher evaporation rate (at the same matric potential) and a longer decreasing period during Stage II evaporation.

2.1.3. The Stage III Evaporation

The Stage III evaporation is therefore the period when vapor diffusion actually controls (Shokri & Or, 2011). As shown in Figure 1c, the vapor conductivity only exceeds the film conductivity when soil water content is extremely low. In this stage, the thin soil surface layer is (almost) completely dried (Figures 1a and 1b), with some tightly bounded thin liquid films left. The soil surface water content is equal to the air-dry value. The evaporation process is accompanied by the receding of vaporization plane (also known as the secondary drying front) into deeper soil. The vapor diffusion-controlled evaporation rate is very low (Figure 1a) and depends on the diffusion length between vaporization plane and soil surface (Shorkri et al., 2011).

2.1.4. The Complete Evaporation Process

By including film flow, the evaporation process can then be summarized into three typical stages as shown in Figure 1d, with, however, some different explanations with the classic theory: (1) The Stage I evaporation is supported by capillary flow from drying front to soil surface. This stage ends when the driving capillary water potential difference between drying front and soil surface cannot overcome the gravitational forces and viscous dissipation, marked by a critical surface water content or a characteristic drying depth (Lehmann et al., 2008). The duration of this stage depends on the width of pore size distribution and is also impacted by the nonlinear boundary layer interactions (Haghighi & Or, 2013; Shahraeeni et al., 2012) as well as the soil texture-dependent capillary flow limitations (Haghighi et al., 2013; Lehmann et al., 2018). When neglecting capillary flow limitations, the evaporation rate is mainly controlled by the atmospheric demand. (2) The Stage II evaporation is also supported by liquid flow, however, in the form of liquid film within a very thin soil surface layer. The capillarity-driven water can no longer achieve the soil surface directly. This stage ends when vapor conductivity becomes dominant over film conductivity, marked with the jump of vaporization plane from surface to deeper soil. The duration of this stage depends mainly on the specific surface area of porous media. The evaporation rate is limited by the soil water transport ability mainly in film form. (3) The Stage III evaporation is the vapor diffusion stage. An almost completely dried layer is developed at the soil surface and it grows deeper when the drying process keeps going. The evaporation rate depends on the depth of the vaporization plane, which is also known as the secondary drying front.

At pore scale (Figure 1d), the end of Stage I evaporation occurs when the air begins to invade the finest pores at the soil surface. During the Stage II evaporation, almost no saturated pores exist at the soil surface, liquid water is mainly retained in the form of film and can move along the surface of porous media. In the Stage III evaporation, almost no liquid water exists in pores and on the soil particle surface except some extremely thin films tightly bounded by adsorption force (depends on the air humidity).

2.2. Model Development

2.2.1. Accounting for Film Flow in the Evaporation Estimation

Under most field atmospheric conditions, the evaporation rate is approximately equal to potential evaporation during Stage I period. In Stage III period, the evaporation rate is very low. Therefore, the key is to define the evaporation rate in Stage II evaporation.

During Stage II period, the evaporation rate is limited by the soil water transport ability, which can be expressed by the Buckingham-Darcy's law, written as

$$\mathrm{LE} = -K(\theta)\frac{dh}{d\theta}\frac{d\theta}{dz}\bigg|_{z=0}, \tag{1}$$

where LE (L T^{-1}) is the actual evaporation rate, and K (L T^{-1}) and h (L) are the hydraulic conductivity and water potential at the surface water content θ, respectively.

When ignoring capillary flow limitations and nonlinear boundary layer interactions, the evaporation rate in Stage I period is equal to the potential evaporation rate, LE_p. Therefore, at the onset of Stage II evaporation, equation (1) becomes

$$\mathrm{LE}_c = -K(\theta_c)\frac{dh}{d\theta}\frac{d\theta}{dz}\bigg|_{z=0,\theta=\theta_c} = \mathrm{LE}_p, \tag{2}$$

with θ_c being the critical surface water content marking the discontinuity of capillary flow. It is roughly close to the so-called residual water content (Lehmann et al., 2008; Or et al., 2013). It should be noted that when capillary flow limitations in relation to fine-textured soils (Haghighi et al., 2013) and/or vapor diffusion through above thin boundary layer in relation to high atmospheric demand (Shahraeeni et al., 2012) become important in Stage I period, no constant evaporation rate stage would be observed and the LE_c might have a value less than LE_p (Lehmann et al., 2018; Or & Lehmann, 2019).

To solve equations (1) and (2), information on the soil hydraulic properties are required. In the literature, the capillary-based models, the van Genuchten (1980)-Mualem (1976) model for instance, are applied (e.g., Saito et al., 2006). This is questionable since the film flow, as discussed previously, is thought to be dominant during Stage II evaporation. According to Campbell and Shiozawa (1992), a linear relationship exists between water content and log-scale water potential under dry conditions so that the soil water retention curve that accounts for film flow can be expressed as (Wang et al., 2016)

$$S_f = \frac{\theta}{\theta_c} = 1 - \frac{\ln(h/h_c)}{\ln(h_0/h_c)}, \tag{3}$$

with S_f being the saturation degree that accounts for film water, and h_c and h_0 are the water potential at θ_c and 0, respectively. As suggested by Schneider and Goss (2012), h_0 can be approximately set to 6.3×10^4 m for soils with different texture properties.

The hydraulic conductivity that accounts for film flow depends on the soil specific surface area (SA) and the film thickness f (Bird et al., 1960), in the form of

$$\frac{K(\theta)}{K(\theta_c)} = \frac{\mathrm{SA}\times f^3}{\mathrm{SA}_c \times f_c^{\,3}}. \tag{4}$$

In general, the specific surface area is kept as constant in film conductivity models (Lebeau & Konrad, 2010; Tuller & Or, 2001; Wang et al., 2017). However, this assumption is not appropriate when film thickness is thicker than the width of parallel plates or when the water film does not cover the entire soil surface under extremely dry conditions. When considering the sole contribution of film flow, an effective surface area can be applied. It was expressed as the water content to film thickness ratio, that is, $\mathrm{SA} = \theta/f$. Since the soil surface water content is very low under Stage II evaporation, only van der Waals forces were considered. The film thickness formula proposed in Iwamatsu and Horii (1996) was applied, written as

$$\frac{f}{f_c} = \left(\frac{h}{h_c}\right)^{-1/3}. \tag{5}$$

Substituting equation (5) and $\mathrm{SA} = \theta/f$ into equation (4) gives

$$K(\theta) = K(\theta_c)S_f\left(\frac{h}{h_c}\right)^{-2/3}. \tag{6}$$

Notably, the impact of modified viscosity on film conductivity under very thin film thickness conditions (Lebeau & Konrad, 2010; Tuller & Or, 2001) was not considered here.

The water content gradient $d\theta/dz$ at soil surface is also required in equations (1) and (2). The Stage II evaporation can be seen as a secondary drying process of a very thin soil layer (with several millimeters in length; see Figure 1b) with uniform initial water content θ_c. Similar to the classic evaporation process as described in Gardner (1959) and in Brutsaert (2014), the upper boundary can be set to a fixed water content, θ_m, which is actually the soil air-dry value. The value depends on the soil texture properties and the environmental conditions. The lower boundary can be set at a fixed depth defined as z_d, with the water content assigned as the surface water content, varying from θ_c to θ_m. When the water potential profile in the thin soil surface layer shows high nonlinearity, the water content profile can be seen as linear under dry conditions (Figure 1b). Therefore, this gradient $d\theta/dz$ is approximately equal to $(\theta - \theta_m)/z_d$.

Dividing equation (1) by equation (2) and with the substitution of $d\theta/dz \approx (\theta - \theta_m)/z_d$ and equations (3) and (6), one obtains

$$\frac{\mathrm{LE}}{\mathrm{LE}_p} = S_f \left(\frac{h}{h_c}\right)^{1/3} \frac{(S_f - S_m)}{(1 - S_m)}. \tag{7}$$

Equation (7) provides a theoretical formula for scaling evaporation rate under Stage II evaporation, with the assumption that film flow dominates the soil surface water flow process. The normalized evaporation rate ranges from 1 at the beginning of Stage II evaporation to 0 when the air-dry soil water content is reached at the end of Stage II evaporation. Note that the impact of vapor diffusion is not considered in equation (7). This film flow-based evaporation rate estimation method is simply termed as the E_FILM model.

The E_FILM model requires the input of soil surface water potential h, which is highly sensitive to water content and depends on soil texture properties. Alternatively, h can be calculated from the well-known Kelvin equation under dry conditions, assuming a thermodynamic equilibrium between liquid and vapor phase. Therefore, h can be written as

$$h = \frac{RT}{Mg} \ln(\mathrm{RH}), \tag{8}$$

where R is the universal gas constant (8.314 J·mol^{-1}·K^{-1}), T (Kelvin) is the absolute temperature, M is the molecular weight of water (0.018015 kg mol^{-1}), g is the gravitational acceleration (9.81 m s^{-2}), and RH is the in-equilibrium relative humidity at soil surface. An illustration in Figure 2a, shows that the temperature effect on water potential estimation is not significant. With neglecting the temperature effect, equation (7), therefore, can be written in the form of RH as

$$\frac{\mathrm{LE}}{\mathrm{LE}_p} = \left[\frac{\ln(\mathrm{RH})}{\ln(\mathrm{RH}_c)}\right]^{1/3} \frac{\ln[\ln(\mathrm{RH}_0)/\ln(\mathrm{RH})]}{\ln[\ln(\mathrm{RH}_0)/\ln(\mathrm{RH}_c)]} \frac{\ln[\ln(\mathrm{RH}_m)/\ln(\mathrm{RH})]}{\ln[\ln(\mathrm{RH}_m)/\ln(\mathrm{RH}_c)]}, \tag{9}$$

where RH_0 is the in-equilibrium relative humidity at the water potential of h_0, being 1.04% at 20 °C, while RH_c and RH_m correspond to the water potential h_c and h_m, respectively.

The merit of using RH is that when vapor pressure is in equilibrium with soil water potential, RH keeps almost constant as 100% during Stage I evaporation since the soil moisture supply is sufficient. It begins to decrease rapidly in Stage II evaporation and then change slowly in Stage III evaporation, reflecting a moisture-limited condition. This change is consistent with the evaporation rate dynamic. Hence, the critical relative humidity RH_c and RH_m can be chosen as the maximum (except the value of 1) and the minimum value of the observed RH, respectively. Tuller and Or (2005) suggested an empirical threshold potential around -10^3 m (corresponding to an RH of 93% at 20 °C) where the capillary condensation becomes negligible. When continuous observation of RH is unavailable, this empirical value is suggested as the critical water potential value for different soils.

Equation (9) provides a scaling method for soil evaporation estimation, requiring RH as the sole input. As shown in Figure 2b, a nonlinear relationship exists between the evaporation rate and the surface water

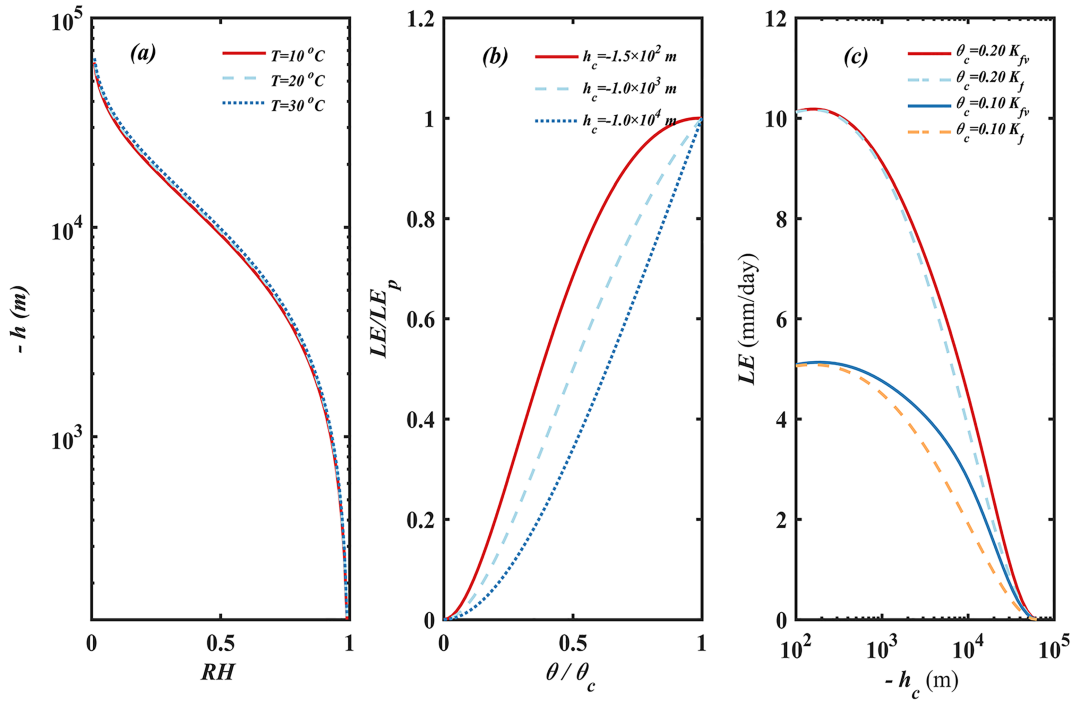

Figure 2. (a) The relationship between water potential and relative humidity under different temperatures. (b) Illustration of the E_FILM model with different critical water potential values; the surface water content is calculated with equation (3). (c) Illustration of the evaporation rate calculated with different critical water content values; the solid line accounts for both film flow and vapor diffusion while the dashed line accounts for film flow only (see Appendix A). The air-dry water content θ_m is set as 0, and the depth of the thin layer z_d is set as 5 mm for illustration.

content. It depends on the critical soil water potential where Stage II evaporation begins. The more negative critical water potential is expected for soils with finer texture under film flow limitations as illustrated in Figure 2c. Notably, here, we did not consider the possible impact of capillary flow limitations. We emphasize here again that the E_FILM model deals with the water flux in a very thin soil surface layer, with only several millimeters in depth. Therefore, much negative matric potential values are expected compared to those observed at deeper layers in the literature.

It is interesting to note that if the surface area SA was kept constant in equation (4), the E_FILM model would have the form of

$$\frac{\mathrm{LE}}{\mathrm{LE}_p} = \frac{S_f - S_m}{1 - S_m}. \tag{10}$$

Equation (10) yields a linear relationship between the scaled evaporation rate and the soil surface water content. It is in the same form as the widely applied but empirically based Bucket model (Budyko, 1974). Hence, equation (10) provides a physical explanation for the Bucket method. The slight difference between equation (10) and the Bucket model is that the soil water content in equation (10) is observed in a depth of several millimeters; while in the Bucket model, it generally represents a depth of several to tens of centimeters. However, the assumption that the water content shows a similar changing trend at different depths (near the soil surface) seems to be appropriate in the drying process.

The difference between equations (7) and (10) comes from the different conductivity functions associated with film flow (equation (4)). In deriving equation (7), only film-form water flow is considered, assuming no contribution comes from capillary flow when water content is less than the critical value θ_c. It represents a very dry condition under which the soil water potential dynamic can usually be captured by changes in RH (Tuller & Or, 2005). When Stage I evaporation ends at a more positive critical water potential (in a magnitude that cannot be captured by RH variation), water flow in the soil surface might be supplied by both

capillary flow (retained in very fine pores) and film flow (along soil particle surface). Under this situation, equation (10) is preferred with the input of soil surface water potential or water content. This is because the constant specific surface area assumption in equation (4) generally yielded a close agreement with observed conductivities in relatively high water potential range (Lebeau & Konrad, 2010; Tuller & Or, 2001; Wang et al., 2017).

2.2.2. The Impact of Capillary Flow Limitations in Stage I Evaporation

In the former section, it is assumed that the capillarity-driven water supply is sufficient to meet the atmospheric water demand in Stage I, therefore, LE is equal to LE_p for surface water content higher than θ_c (equation (2)). However, when the capillary flow limitations become important in relation to fine-textured soils (Haghighi et al., 2013; Lehmann et al., 2018; Or & Lehmann, 2019) and/or the vapor diffusion limitations through the above thin boundary layer is significant under high atmospheric demand (Shahraeeni et al., 2012), LE may also show a falling trend and be less than LE_p during Stage I period.

Under this situation, the resistances come from capillary flow, film flow, as well as vapor diffusion should be taken into account together to describe a complete soil evaporation process. Haghighi et al. (2013) and more recently, Lehmann et al. (2018) provided a formula for describing the capillary limitations on evaporation rate. By estimating LE_c in equation (2) with this formula, the evaporation rate dynamics during both Stage I and Stage II period may be described. Such combination method, however, requires a detail parameterization of soil hydraulic properties and involves a lot of uncertainty. For example, due to the high specific surface area, the film flow may be important even in Stage I period for fine-textured soils. This possible impact however was not taken into account in the existing theory that deals with capillary limitations (e.g., Haghighi et al., 2013; Lehmann et al., 2018). In the present study, therefore, we focus solely on the limitations that come from film flow in Stage II period and ignore the possible impact of capillary flow limitations in Stage I period.

2.2.3. The Impact of Vapor Flow

Equation (7) considers film flow only and ignores the potential impact of vapor transport that is dominant during Stage III evaporation. Here, the isothermal vapor flow is included to evaluate its influence on the evaporation rate. The vapor diffusion contribution is calculated following the classical theory as provided in Philip and de Vries (1957) and in Saito et al. (2006). The detail is presented in Appendix A. It should be noted that only isothermal vapor diffusion is considered so that the impact of temperature gradient is not included.

Figure 2c shows that the contribution of vapor flow is, in general, much less than that of film flow. It is only important for soils with coarse texture and for very dry conditions. Considering vapor flow in soil evaporation estimation, however, will produce a very complex formula and requires additional information related to specific soil properties. Here, we suggest a simple equation to include the impact of vapor flow, written as

$$\mathrm{LE} = S_f\left(\frac{h}{h_c}\right)^{1/3}\frac{(S_f - S_m)}{(1 - S_m)}\left(\mathrm{LE}_p - \mathrm{LE}_v\right) + \mathrm{LE}_v, \tag{11}$$

where LE_v represents the contribution from vapor flow. Shokri and Or (2011) showed that the vapor diffusion flux was quite similar for soils with different texture, often in a range from 0.5 to 2.5 mm d^{-1} at the onset of Stage III evaporation. The mean vapor diffusion rate is about 1.5 mm d^{-1} for different soils. The accurate estimation of vapor diffusion rate, however, requires the length between the vaporization plane and the soil surface and requires also the atmospheric vapor pressure. Equation (11) is only suggested when vapor flow is believed to be important.

2.2.4. Evaporation Rate Estimation in Field

When it comes to field scale, the soil evaporation estimation becomes more complicated. In contrast with the monotonically increase of the film-dominated soil layer thickness as in the laboratory experiment, the thin layer thickness under real field conditions would grow and reduce during daytime and nighttime due to the soil moisture redistribution (Brutsaert, 2014). As a result, a distinct diurnal pattern of evaporation rate would be observed in field (e.g., Idso et al., 1974, 1979; Jackson et al., 1976). However, when considering the evaporation process at the daily scale, this diurnal patter can be avoided (Brutsaert, 2014). The vapor transport can also be neglected for its minor effect on the daily evaporation rate (e.g., Milly, 1984a, 1984b; Saravanapavan & Salvucci, 2000).

Table 1
The Laboratory Evaporation Tests from Wilson (1990) and Zhang et al. (2015)

Test no.	Soil type	Sample thickness (mm)	RH of air	Reference
Sand_1	Beaver	0.7	0.53	Wilson
Sand_2	Creek	0.5	0.44	(1990)
Sand_3	Sand	0.5	0.58	
Silt_1	Custom	0.5	0.21	Wilson
Silt_2	Silt	0.3	0.39	(1990)
Silt_3		0.3	0.62	
Clay_1	Regina	0.7	0.39	Wilson
Clay_2	Clay	0.3	0.35	(1990)
Clay_3		0.2	0.50	
Soil column	Medium Sand	500	0.50	Zhang et al. (2015)

Abbreviation: RH = relative humidity.

Another difficulty with field data is that the relative humidity is often observed at the height of 2 m above the soil surface, which might not be in equilibrium with soil surface. However, the relative humidity at different heights generally shows a similar trend during the evaporation process. Equation (9) shows that it is the log(RH)/log(RH_c) ratio that controls the value of LE. Therefore, it might be appropriate to assume that the ratio of log-scale relative humidity at soil surface can be represented by that observed at the height of 2 m. However, unlike laboratory experiments, it is hard to define the critical RH_c where the evaporation rate begins to decrease as the (atmospheric) boundary condition is an open system. In this study, a maximum value of 0.85 derived by trial and error is suggested as the upper boundary for the critical RH_c. That is, RH_c is the minimum value between 0.85 and the observed maximum RH. RH_m is simply set to the minimum value of the observed RH. This requires the observations to cover a complete drying period. The influence of the soil heterogeneity here is simplified by assuming that the applied air relative humidity represents a mixture of soil surface moisture conditions.

With these assumptions and by ignoring vapor flow, Equation (9) can now be used to estimate the field soil evaporation rate, requiring only the meteorological data as input. In this study, the potential evaporation rate LE_p is calculated by the Priestley and Taylor (1972) equation, written as

$$LE_p = \alpha_{PT}\frac{\Delta}{\Delta+\gamma}(R_n - G), \tag{12}$$

where α_{PT} is the Priestley-Taylor constant, with the value of 1.26; Δ (kilopascal per Kelvin) is the slope of the vapor pressure curve at air temperature; γ (kilopascal per Kelvin) is the psychrometric constant, R_n (watt per square meter) is the net radiation, and G (watt per square meter) is the soil heat flux.

3. Data Description

3.1. Data From Laboratory Experiment

The proposed E_FILM model is evaluated at both laboratory and field scales. The laboratory data include nine thin (less than 1 mm in length) soil evaporation experiments provided in Wilson (1990) and one thick soil column (50 cm in length) evaporation experiment presented in Zhang et al. (2015).

Table 2
Flux Sites Including Bare-Soil Periods, Modified from Merlin et al. (2016)

Site	Exp./Net.	Latitude; longitude	Land cover	Soil texture	Reference
AUStu	OzFlux	−17.15; 133.35	Grass	Silt loam	Beringer et al. (2011)
BELon	GHGEurope	50.55; 4.74	Crop	Silt loam	Papale et al. (2006)
CHOe2	GHGEurope	47.29; 7.73	Crop	Silty clay	Alaoui and Goetz (2008)
DEGeb	GHGEurope	51.10; 10.91	Crop	Silty clay loam	Kutsch et al. (2010)
ESES2	GHGEurope	39.28; −0.32	Crop	Silty clay	Kutsch et al. (2010)
FRAur	GHGEurope	43.55; 1.11	Crop	Clay loam	Béziat et al. (2009)
FRAvi	GHGEurope	43.92; 4.88	Crop	Silty clay loam	Garrigues et al. (2014)
FRLam	GHGEurope	43.50; 1.24	Crop	Clay	Béziat et al. (2009)
ITBCi	GHGEurope	40.52; 14.96	Crop	Clay	Denef et al. (2013)
NIHAP	HAPEX	2.24; 13.20	Bare	Sand	Wallace et al. (1993)
USArm	AmeriFlux	36.61; −97.49	Crop	Clay	Fischer et al. (2007)
USDk1	AmeriFlux	35.97; −79.09	Grass	Loam	Novick et al. (2004)
USFwf	AmeriFlux	35.45; −111.77	Grass	Silt loam	Dore et al. (2012)
USIb1	AmeriFlux	41.86; −88.22	Crop	Silty clay loam	Wu et al. (2012)
USIHO	IHOP	36.47; 100.62	Bare	Sandy clay loam	Lemone et al. (2007)

Abbreviation: IHOP = International H2O Project; Hapex = Hydrology-Atmosphere Pilot Experiment.

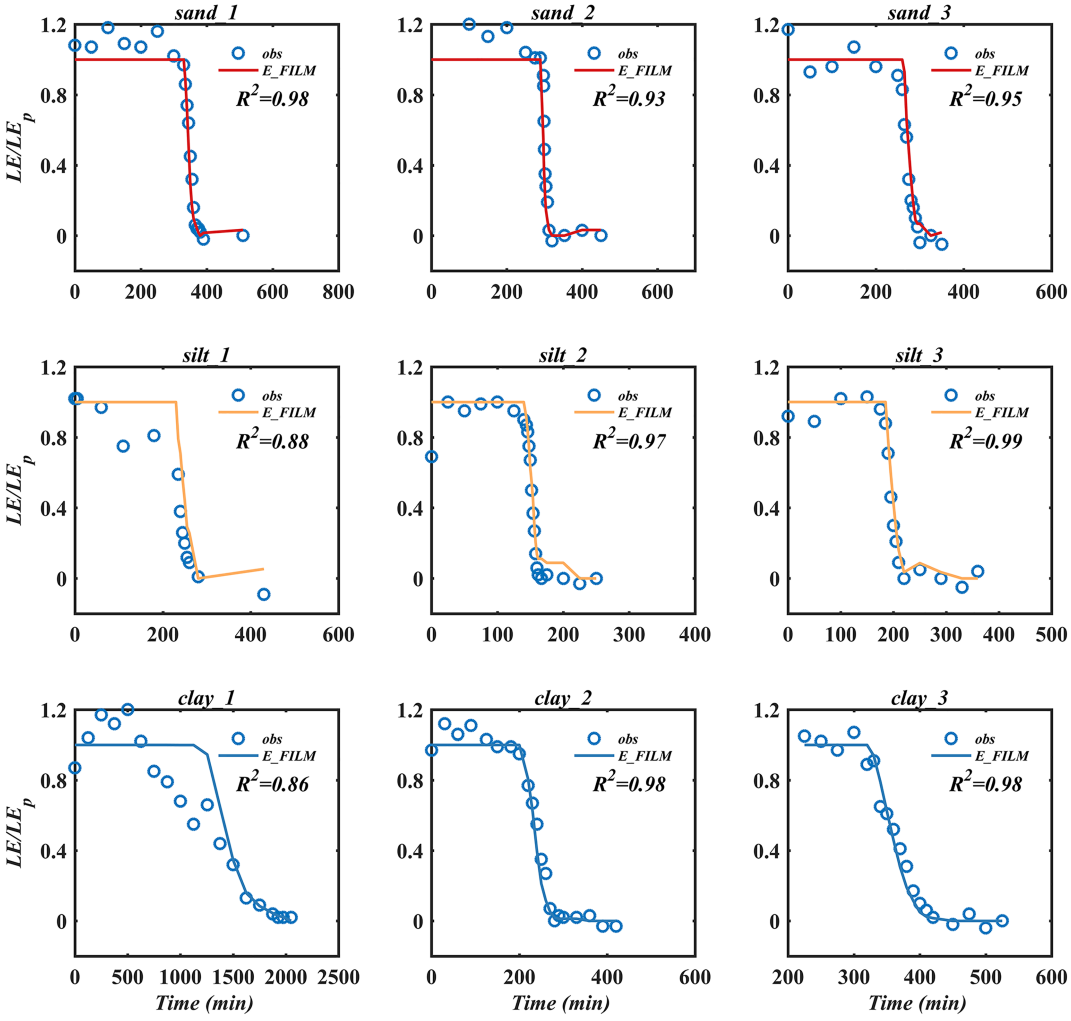

Figure 3. E_FILM model testing with thin soil evaporation experiments from Wilson (1990), including sand, silt, and clay.

The thin soil evaporation test includes three soil types: Beaver Creek Sand, Custom Silt, and Regina Clay. For each soil type, three tests were presented (see Table 1). In all tests except for tests silt_1 and clay_1, the thin soil samples were prepared by gently dusting a layer of dry soil onto a sheet of aluminum foil. The sample was then saturated with distilled water using a mist applicator. For tests silt_1 and clay_1, the soil sample was prepared as slurry and poured into the evaporation pan to achieve a thicker soil layer. As described in Wilson (1990), some difficulties were encountered when using the slurried soil method. For example, non-uniform drying was found for silt_1 test and for clay_1 test. Besides, shrinking and deformation were frequently observed for clay_1 test, which resulted in problems such as curling and irregular drying. The evaporation was preceded in room temperature, and the relative humidity of air was kept almost constant. For the details, please refer to Wilson (1990).

The thick soil evaporation experiment was provided in Zhang et al. (2015). The soil column was 50 cm in length. Different from the thin soil evaporation, an infrared lamp was used for supplying heat to soil surface. The relative humidity near soil surface was recorded during the drying process. The experiment details can be seen in Zhang et al. (2015).

3.2. Data Collected From Field Sites

The field sites are chosen from the collection presented in Merlin et al. (2016), including 15 sites representing bare-soil conditions across different countries (see Table 2). Note that only sites with more than 40 days of observation are selected. These sites were selected mostly from the national and international flux station networks (OZnet, European Flux Database, and AmeriFlux) while two sites were chosen from short-term

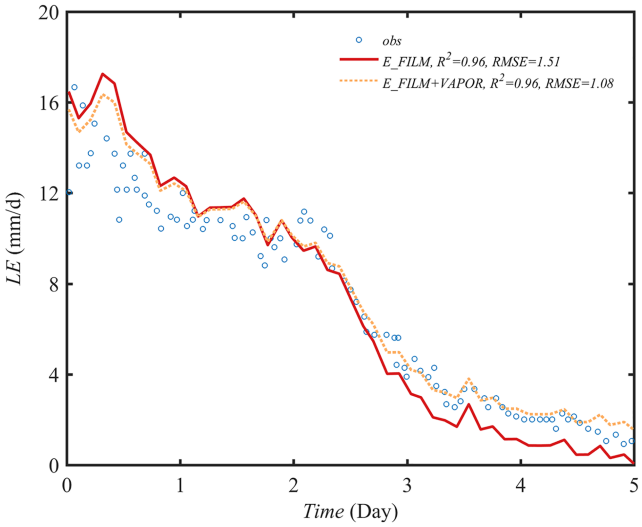

Figure 4. E_FILM model testing with thick sand column evaporation experiment from Zhang et al. (2015).

intensive field campaigns such as the Hydrology-Atmosphere Pilot Experiment and International H_2O Project. Most of these sites, however, are not under true bare-soil conditions. Merlin et al. (2016) provided a principle for choosing the "bare soil" period where plant transpiration is thought to be negligible. For more details, please refer to Merlin et al. (2016).

4. Results and Discussion

4.1. Model Testing With Thin Soil Evaporation

The thin soil evaporation presented in Wilson (1990) represents exactly the physical process described by the E_FILM model, that is, a drying process of extremely thin (less than 1 mm) soil layer. Hence, there exists no impact of moisture supply from below soil as in thick soil column evaporation. The vapor flow within soil can be neglected because there is no moisture supply during Stage III evaporation. The soil water potential was calculated from observed water content by the measured soil water retention curve. The in-equilibrium relative humidity at soil surface is then provided according to the Kelvin equation. Therefore, these thin soil evaporation experiments provide the perfect data for model testing.

Model testing results as shown in Figure 3 demonstrated clearly that the provided E_FILM model was in excellent agreement with observations for almost all nine experiments. Two exceptions are for tests silt_1 and clay_1, where the evaporation rate began to decrease while the observed RH kept constant as 1. As demonstrated in section 3.1, these two tests applied a different method for sample preparation and yielded a nonuniform drying process. This may explain the mismatch between model predictions and observations.

Another mismatch was observed during Stage I evaporation, where the observed soil evaporation was generally larger than the potential rate. In this experiment, the potential evaporation rate was observed from free water evaporation under the same environment. Therefore, this mismatch may be due to the different vapor diffusion through the thin atmospheric layer above soil and water surface, respectively. This issue is not in the scope of the E_FILM model.

When using E_FILM model to predict the evaporation rate, only in-equilibrium RH and potential evaporation rate LE_p are needed, requiring no adjustable parameter in relation to soil texture. The different evaporation rate changes among different soils have already been captured by the in-equilibrium RH. According to Figure 2c, the critical matric potential is expected to be smaller (more negative) for soils with finer texture under film flow limitations situation. On the contrary, the observed RH_c was close to 0.99 (corresponding to a water potential of −138 m at 20 °C) for all soils. This may be explained by that the critical matric potential that marks the beginning of Stage II evaporation is too large (higher than −138 m for all soils) to be captured by RH observations. This is consistent with the description of the evaporation process in section 2.1, where the critical water potential is thought to be close to the value in corresponding to the residual water content. In the literature (e.g., Wang et al., 2016, 2017), this value was generally higher than −138 m, especially for soils with coarse texture. Nevertheless, as soon as the soil water supply cannot meet the atmospheric demand, the soil surface water potential would decrease dramatically to very negative values, resulting in a decrease of observed RH.

4.2. Model Testing with Soil Column Evaporation

The sand column evaporation experiment presented in Zhang et al. (2015) was undertaken with an external heat supply, resulting in lower RH observations near soil surface, changing from 18% to 58%. Therefore, the soil water potential may not be in equilibrium with the observed RH. However, as discussed previously, it is the h/h_c ratio that controls the change of evaporation rate, and the observed RH can then be used for predicting the evaporation rate. Besides, with external heat supply, the atmospheric demand was very high through the drying process. A decreasing evaporation rate was observed during Stage I period (Figure 4). This might

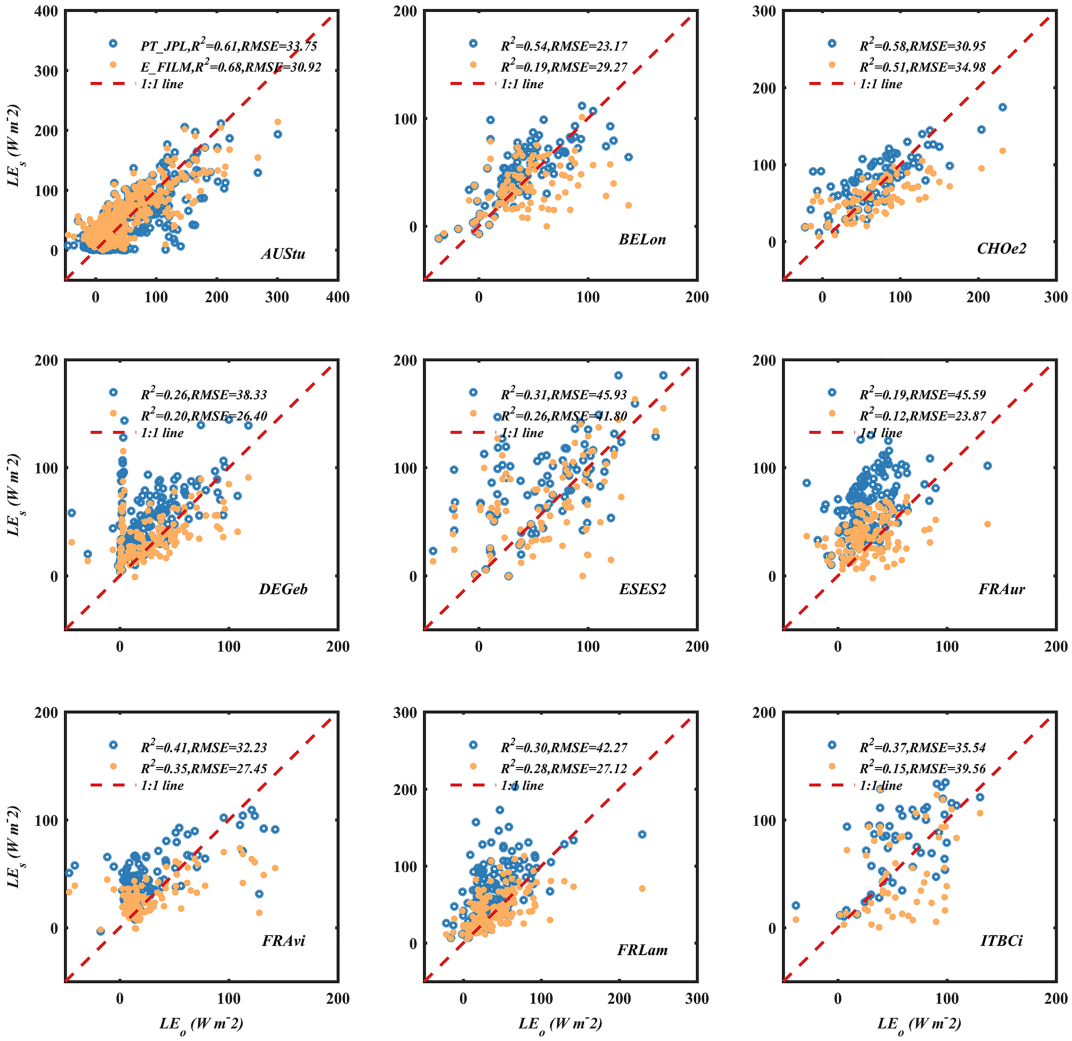

Figure 5. Predicted evaporation flux with the E_FILM model and the Priestley and Taylor Jet Propulsion Laboratory model in the first nine field sites, LE_0 and LE_s are the observed and the simulated evaporation rate, respectively.

be attributed to the vapor diffusion limitations through above thin boundary layer (Shahraeeni et al., 2012). This effect is not included in the E_FILM model development. Therefore, we only considered the drying process after Stage I period, and the critical RH_c was chosen at Day 2 from RH observations.

Figure 4 showed that the estimated evaporation rate was generally in good agreement with observations. An underestimation however was found in the low evaporation rate range. Different from the thin soil evaporation, the vapor flow can be important in the soil column evaporation case, especially during Stage III evaporation. By including vapor flow and by setting LE_v to 1.5 mm d^{-1} (the mean vapor diffusion rate from Shokri & Or, 2011) in equation (11), the model estimation was in excellent agreement with observations (after 2 days).

Here, no enhancement factor in relation to vapor diffusion is included (Shokri & Or, 2011). The close agreement with observations when considering both film flow and isothermal vapor diffusion might indicate that the unclearly defined enhancement factor (e.g., Saito et al., 2006) actually represents the impact of film flow. However, more testing with different soil columns is needed.

The excellent agreement with the observations of both thin soil and thick soil column evaporation revealed that the E_FILM model (without adjustable parameter) might have captured the actual physical mechanism during Stage II evaporation.

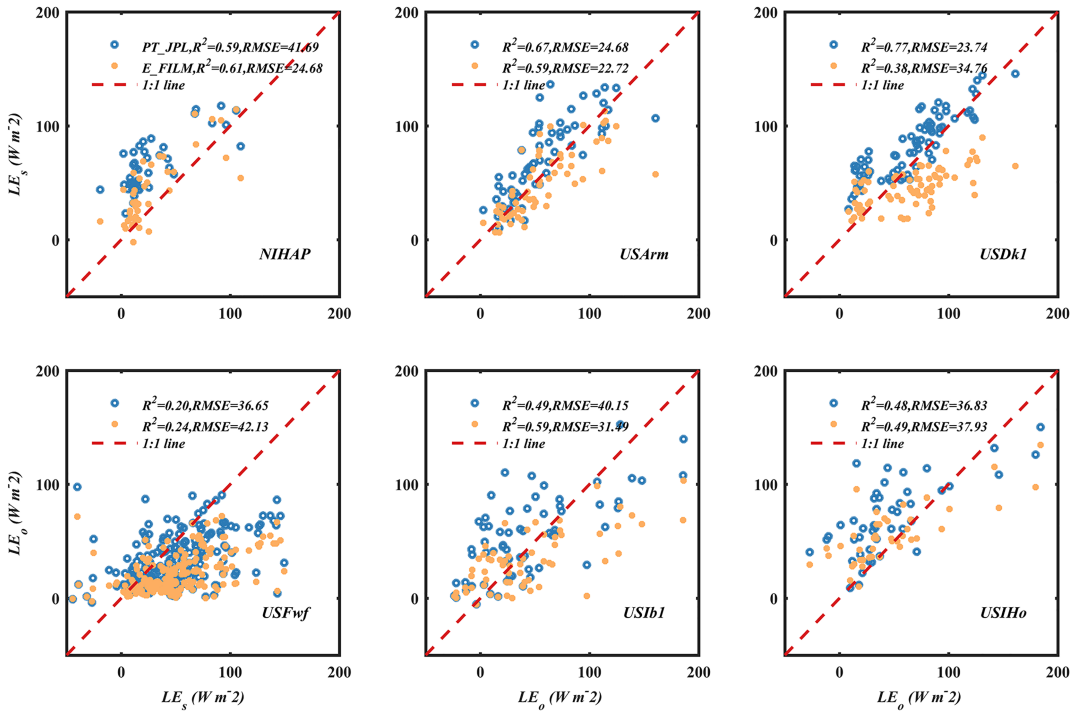

Figure 6. Predicted evaporation flux with the E_FILM model and the Priestley and Taylor Jet Propulsion Laboratory model in last six field sites, LE0 and LEs are the observed and the simulated evaporation rate, respectively.

4.3. Model Testing With Field Observations

When testing the E_FILM model with field observations, significant uncertainties are visible. The main reason is the lack of RH observations at the soil surface. When using the RH observed at 2 m instead, it is difficult to define the critical RH_c as the humidity is not only impacted by soil wetness but also by other atmospheric factors. Under wet conditions, the RH at soil surface is generally higher than that at 2 m above; and therefore, the critical RH_c when using observations at 2 m should have a value smaller than that (close to 0.99) observed in the laboratory. In this study, a maximum value of 0.85 derived by trial and error is suggested as the upper boundary for the critical RH_c. For model illustration, the soil evaporation module from the widely applied Priestley and Taylor Jet Propulsion Laboratory (PT-JPL) model (Fisher et al., 2008) was chosen for comparison. This module uses an empirical equation to express the water stress, also as a function of RH (see Appendix B).

Model testing with 15 sites as shown in Figures 5 and 6 demonstrated that the E_FILM model generally captured the dynamics of evaporation observations. Especially, the E_FILM model improved the prediction under low evaporation conditions in comparison with the PT-JPL model, as shown at sites DEGeb, FRAur, FRAvi, FRLam, and NIHAP. The overestimation of evapotranspiration rates under arid and semiarid sites was known to be a common problem in almost all evapotranspiration models (e.g., Michel et al., 2016). Therefore, the developed E_FILM model may provide a possible solution for this problem.

The E_FILM model underestimated evaporation rate at sites BElon, USDK1, and USFwf. This underestimation can be improved by choosing a lower RH_c, indicating that the critical value is actually different under different conditions.

To summarize, the E_FILM model generally yielded lower root-mean-square errors in comparison with the PT-JPL model, with a mean value of 31.67 and 35.43 W m^{-2}, respectively (Figures 5 and 6). For R^2, however, the PT-JPL model generally presented higher values, with a mean value of 0.45 compared to the 0.38 of the E_FILM model. This much lower R^2 with the E_FILM model was mainly due to the poor performance at sites BELon and USDK1.

The relatively poor performance with field observations might be due to two main reasons. First, most testing sites were not in a true bare-soil situation. As shown in Table 2, only two sites (NIHAP and USIHO) were under bare-soil condition while the observations from other sites were chosen from a "bare soil" period assuming plant transpiration was "negligible or small compared to soil evaporation" (Merlin et al., 2016). However, without direct measurement of the soil evaporation, it is hard to evaluate the data quality. Second, high uncertainty existed in relation to the RH input. In this study, the RH data used were observed at 2 m above the soil surface and should be different from the in-equilibrium RH at the soil surface. Besides, an upper boundary of 0.85 was set for the critical RH_c in this study. However, as discussed previously, this value might be different at different sites. For example, the underestimation at sites BELon and USDK1 can be improved by setting a lower critical RH_c. However, it was hard to define the actual RH_c since this value was not only related to soil texture but also to atmospheric conditions. Uncertainty also existed in defining RH_m. In this study, RH_m was simply set as the lowest value of the observed RH. This principle was appropriate only when the observations covered a complete drying period. Note that the impacts of RH_c and RH_m are highly correlated in the E_FILM model.

In spite of this disadvantage, the E_FILM model was attractive for its solid physical base, which was evidenced by laboratory observations. Moreover, the estimation of soil evaporation in field showed an improvement under dry conditions. The film-dominant assumption in the E_FILM model was also consistent with the field drying experiment in Goss and Madliger (2007), where they found that the film flow has a significant contribution in soil evaporation. However, further work is needed to derive a complete evaporation rate estimation model by including both capillary and film limitations and to improve the model performance in field, for example, considering the input of soil surface water content.

5. Conclusions

This study provided a new interpretation of the typical soil evaporation process by including the impact of film flow along the soil particle surface. This film flow was usually thought to be unimportant and then neglected in soil drying process (e.g., Idso et al., 1974; Philip & de Vries, 1957). However, recent progress in soil hydraulic modeling development confirmed this film flow as a dominant process under low moisture conditions (e.g., Peters, 2013; Tuller & Or, 2001; Wang et al., 2016, 2017, 2018). By including this film flow, the typical drying process was revisited. The result found that this film flow might be the dominant process for limiting the evaporation loss under Stage II evaporation, in which the vapor flow was usually regarded as the limitation factor (e.g., Lehmann et al., 2008; Or et al., 2013; Philip & de Vries, 1957; Saito et al., 2006). The typical evaporation process was then interpreted as the capillary flow-supported Stage I evaporation, the film flow-controlled Stage II evaporation, and the vapor diffusion-dominant Stage III evaporation.

Based on the assumption that film flow controlled the Stage II evaporation, a physically based model was developed by parameterizing the Buckingham-Darcy's law. The model provided a solid basis for describing the moisture limitation on evaporation rate, requiring only meteorological data as input and introducing no adjustable parameter. The impact of vapor flow was also discussed. It was found to be only important for soils with coarse texture under very dry conditions.

Model testing with laboratory data, including nine thin soil thickness evaporation tests and one thick sand column evaporation, yielded excellent agreement with observations. The model evaluation with 15 field sites, however, introduced some uncertainty. The main reason is the lack of in-equilibrium relative humidity observations near the soil surface. Nevertheless, the proposed E_FILM model significantly improves the performance under dry conditions in comparison with the widely applied PT-JPL model. Since the evaporation overestimation in arid and semiarid regions has been found in almost all evapotranspiration estimation models (Michel et al., 2016), this E_FILM model provides an opportunity to improve the evaporation estimation under such dry conditions. However, the present E_FILM model did not consider the impact of capillary limitations, which might be important in fine-textured soils (Haghighi et al., 2013; Lehmann et al., 2018), and further work is needed to test and improve the model performance in field, especially in relation to the determination of the critical RH_c that marks the beginning of Stage II evaporation.

Appendix A

When both film flow and vapor diffusion are included, the evaporation rate can be expressed by parameterizing the Buckingham-Darcy's law (equation (7)) as

$$\mathrm{LE}\approx\left(K_f+K_v\right)h\ln\left(\frac{h_0}{h_c}\right)\frac{\left(S_f-S_m\right)}{z_d}, \tag{A1}$$

where K_f and K_v are the hydraulic conductivity that accounts for film flow and isothermal vapor flow, respectively.

By applying the effective surface area, the film conductivity is expressed as

$$K_f=\frac{2\rho g\theta_f}{3\pi\eta}f^2, \tag{A2}$$

where ρ is the water density (9.98×10^2 kg m^{-3}), g is the acceleration of gravity (9.81 m s^{-2}), η is fluid viscosity (1.005×10^{-3} Pa s at 293 K), and the film thickness f is expressed following Tuller and Or (2001) as

$$f=\sqrt[3]{\frac{-A_{\mathrm{svl}}}{6\ \pi\ \rho gh}}, \tag{A3}$$

where A_{svl} is the Hamaker constant for solid-vapor interactions through the intervening liquid and is set as -6.0×10^{-20} J following Tuller and Or (2001).

The isothermal vapor conductivity is given in Saito et al. (2006) as

$$K_v=\frac{\rho_v}{\rho}D\frac{Mg}{RT}\mathrm{RH}, \tag{A4}$$

where ρ_v (kilogram per cubic meter) is the saturated vapor density and D (square meter per second) is the vapor diffusivity, written as

$$D=\tau\theta_aD_a, \tag{A5}$$

with θ_a being the air-filled porosity, τ the tortuosity factor calculated according to Millington and Quirk (1961) as

$$\tau=\frac{{\theta_a}^{7/3}}{{\theta_s}^2}, \tag{A6}$$

with θ_s the saturated water content.

And D_a is the vapor diffusivity in air, written as

$$D_a=2.12\times10^{-5}\left(\frac{T}{273.15}\right)^2. \tag{A7}$$

Appendix B.

The soil evaporation in the PT-JPL model (Fisher et al., 2008) is estimated by

$$\mathrm{LE}=\mathrm{RH}^{\mathrm{VPD}/\beta}\mathrm{LE}_p, \tag{B1}$$

with VPD (kilopascal) being vapor pressure deficit, and β (1.0 kPa) representing the relative sensitivity to VPD.

Acknowledgments

The research was supported by the National Natural Science Foundation of China (41601030) and the National Key Research and Development Program of China (2017YFC0406105) and the Fundamental Research Funds for Central Universities, China University of Geosciences (Wuhan; CUG1323531877). The laboratory data are collected from the doctoral thesis of Graham W. Wilson (University of Kansas) and from the research of Chenming Zhang (University of Queensland), both are greatly acknowledged. The original field bare-soil data set was prepared in the frame of the MIXMOD-E project (ANR-13-JS06-0003). We acknowledge the following sites of the European Flux Database (BELon, CHOe2, DEGeb, ESES2, FRAur, FRAvi, FRLam, and ITBCi), the following AmeriFlux sites (USArm, USDk1, and USFwf), the following OzFlux site (AUStu), and the following short-term intensive field campaigns (HAPEX-Sahel and IHOP) for their data records. Data are available on repository (https://doi.org/10.6084/m9.figshare.8898923). Finally, the authors thank the editor, the associate editor, and all anonymous reviewers for their very insightful and constructive comments on this manuscript.

References

Alaoui, A., & Goetz, B. (2008). Dye tracer and infiltration experiments to investigate macropore flow. *Geoderma*, *144*(1-2), 279–286.

Barton, I. J. (1979). A parameterization of the evaporation from nonsaturated surfaces. *Journal of Applied Meteorology*, *18*(1), 43–47.

Beringer, J., Hacker, J., Hutley, L. B., Leuning, R., Arndt, S. K., Amiri, R., et al. (2011). SPECIAL—Savanna patterns of energy and carbon integrated across the landscape. *Bulletin of the American Meteorological Society*, *92*(11), 1467–1485. https://doi.org/10.1175/2011BAMS2948.1

Béziat, P., Ceschia, E., & Dedieu, G. (2009). Carbon balance of a three crop succession over two cropland sites in South West France. *Agricultural and Forest Meteorology*, *149*(10), 1628–1645.

Bird, R. B., Stewart, W. E., & Lightfoot, E. N. (1960). *Transport Phenomena*. New York: John Wiley.

Brutsaert, W. (2005). *Hydrology: An introduction*. Cambridge University Press.

Brutsaert, W. (2014). Daily evaporation from drying soil: Universal parameterization with similarity. *Water Resources Research*, *50*, 3206–3215. https://doi.org/10.1002/2013WR014872

Budyko, M. I. (1974). *Climate and life*. New York, NY: Academic Press.

Campbell, G. S., & Shiozawa, S. (1992). Prediction of hydraulic properties of soils using particle-size distribution and bulk density data. In M. T. van Genuchten, F. J. Leij, & L. J. Lund (Eds.), *Proceedings of the international workshop on indirect methods for estimating the hydraulic properties of unsaturated soil* (pp. 317–328). Riverside, CA, USA: University of California.

Chen, P., & Pei, D. C. T. (1989). A mathematical model of drying processes. *International Journal of Heat and Mass Transfer*, *32*(2), 297–310.

Corey, A. T., & Brooks, R. H. (1999). The Brooks-Corey relationships. In M. T. van Genuchten, F. J. Leij, & L. Wu (Eds.), *Proceedings of the international workshop on characterization und measurement of the hydraulic properties of unsaturated porous media* (pp. 13–18). Riverside, CA: University of California.

Deardorff, J. (1977). A parameterization of ground-surface moisture content for use in atmospheric prediction models. *Journal of Applied Meteorology*, *16*(11), 1182–1185.

Denef, K., Del Galdo, I., Venturi, A., & Cotrufo, M. F. (2013). Assessment of soil C and N stocks and fractions across 11 European soils under varying land uses. *Open Journal of Soil Science*, *3*(07), 297.

Dickinson, R. E. (1984). Modeling evapotranspiration for three-dimensional global climate models. *Climate Processes and Climate Sensitivity*, *29*, 58–72.

Dore, S., Montes-Helu, M., Hart, S. C., Hungate, B. A., Koch, G. W., Moon, J. B., et al. (2012). Recovery of ponderosa pine ecosystem carbon and water fluxes from thinning and stand-replacing fire. *Global Change Biology*, *18*(10), 3171–3185. https://doi.org/10.1111/j.1365-2486.2012.02775.x

Dorman, J. L., & Sellers, P. J. (1989). A global climatology of albedo, roughness length and stomatal resistance for atmospheric general circulation models as represented by the Simple Biosphere Model (SiB). *Journal of Applied Meteorology*, *28*(9), 833–855.

Fischer, M. L., Billesbach, D. P., Berry, J. A., Riley, W. J., & Torn, M. S. (2007). Spatiotemporal variations in growing season exchanges of CO2, H2O, and sensible heat in agricultural fields of the Southern Great Plains. *Earth Interactions*, *11*(17), 1–21.

Fisher, J. B., Melton, F., Middleton, E., Hain, C., Anderson, M., Allen, R., et al. (2017). The future of evapotranspiration: Global requirements for ecosystem functioning, carbon and climate feedbacks, agricultural management, and water resources. *Water Resources Research*, *53*, 2618–2626. https://doi.org/10.1002/2016WR020175

Fisher, J. B., Tu, K. P., & Baldocchi, D. D. (2008). Global estimates of the land–atmosphere water flux based on monthly AVHRR and ISLSCP-II data, validated at 16 FLUXNET sites. *Remote Sensing of Environment*, *112*(3), 901–919.

Fredlund, D. G., & Xing, A. Q. (1994). Equations for the soil-water characteristic curve. *Canadian Geotechnical Journal*, *31*(4), 521–532.

Gardner, W. R. (1959). Solutions of the flow equation for the drying of soils and other porous media 1. *Soil Science Society of America Journal*, *23*(3), 183–187.

Garrigues, S., Olioso, A., Calvet, J. C., Martin, E., Lafont, S., Moulin, S., et al. (2014). Evaluation of land surface model simulations of evapotranspiration over a 12 year crop succession: Impact of the soil hydraulic properties. *Hydrology and Earth System Sciences Discussions*, *11*(10), 11,687–11,733.

Goss, K. U., & Madliger, M. (2007). Estimation of water transport based on in situ measurements of relative humidity and temperature in a dry Tanzanian soil. *Water Resources Research*, *43*, W05433. https://doi.org/10.1029/2006WR005197

Gu, C., Ma, J., Zhu, G., Yang, H., Zhang, K., Wang, Y., & Gu, C. (2018). Partitioning evapotranspiration using an optimized satellite-based ET model across biomes. *Agricultural and Forest Meteorology*, *259*, 355–363.

Haghighi, E., & Or, D. (2013). Evaporation from porous surfaces into turbulent airflows: Coupling eddy characteristics with pore scale vapor diffusion. *Water Resources Research*, *49*, 8432–8442. https://doi.org/10.1002/2012WR013324

Haghighi, E., Shahraeeni, E., Lehmann, P., & Or, D. (2013). Evaporation rates across a convective air boundary layer are dominated by diffusion. *Water Resources Research*, *49*, 1602–1610. https://doi.org/10.1002/wrcr.20166

Haghighi, E., Short Gianotti, D. J., Akbar, R., Salvucci, G. D., & Entekhabi, D. (2018). Soil and atmospheric controls on the land surface energy balance: A generalized framework for distinguishing moisture-limited and energy-limited evaporation regimes. *Water Resources Research*, *54*, 1831–1851. https://doi.org/10.1002/2017WR021729

Idso, S. B., Reginato, R. J., & Jackson, R. D. (1979). Calculation of evaporation during the three stages of soil drying. *Water Resources Research*, *15*(2), 487–488.

Idso, S. B., Reginato, R. J., Jackson, R. D., Kimball, B. A., & Nakayama, F. S. (1974). The three stages of drying of a field soil 1. *Soil Science Society of America Journal*, *38*(5), 831–837.

Iwamatsu, M., & Horii, K. (1996). Capillary condensation and adhesion of two wetter surfaces. *Journal of colloid and interface science*, *182*(2), 400–406.

Jackson, R. D., Idso, S. B., & Reginato, R. J. (1976). Calculation of evaporation rates during the transition from energy-limiting to soil-limiting phases using albedo data. *Water Resources Research*, *12*(1), 23–26.

Kutsch, W. L., Aubinet, M., Buchmann, N., Smith, P., Osborne, B., Eugster, W., et al. (2010). The net biome production of full crop rotations in Europe. *Agriculture, Ecosystems & Environment*, *139*(3), 336–345. https://doi.org/10.1016/j.agee.2010.07.016

Lebeau, M., & Konrad, J.-. M. (2010). A new capillary and thin film flow model for predicting the hydraulic conductivity of unsaturated porous media. *Water Resources Research*, *46*, W12554. https://doi.org/10.1029/2010WR009092

Lehmann, P., Assouline, S., & Or, D. (2008). Characteristic lengths affecting evaporative drying of porous media. *Physical Review E*, *77*(5).

Lehmann, P., Merlin, O., Gentine, P., & Or, D. (2018). Soil texture effects on surface resistance to bare-soil evaporation. *Geophysical Research Letters*, *45*, 10–398. https://doi.org/10.1029/2018GL078803

LeMone, M. A., Chen, F., Alfieri, J. G., Cuenca, R. H., Hagimoto, Y., Blanken, P., et al. (2007). NCAR/CU surface, soil, and vegetation observations during the International H2O Project 2002 field campaign. *Bulletin of the American Meteorological Society*, *88*(1), 65–82.
Mahfouf, J. F., & Noilhan, J. (1991). Comparative study of various formulations of evaporations from bare soil using in situ data. *Journal of Applied Meteorology*, *30*(9), 1354–1365.
Mahrt, L., & Pan, H. (1984). A two-layer model of soil hydrology. *Boundary-Layer Meteorology*, *29*(1), 1–20.
Martens, B., Gonzalez Miralles, D., Lievens, H., Van Der Schalie, R., De Jeu, R. A., Fernández-Prieto, D., et al. (2017). GLEAM v3: Satellite-based land evaporation and root-zone soil moisture. *Geoscientific Model Development*, *10*(5), 1903–1925.
Maxwell, R. M., & Condon, L. E. (2016). Connections between groundwater flow and transpiration partitioning. *Science*, *353*(6297), 377–380.
Merlin, O., Olivera-Guerra, L., Hssaine, B. A., Amazirh, A., Rafi, Z., Ezzahar, J., et al. (2018). A phenomenological model of soil evaporative efficiency using surface soil moisture and temperature data. *Agricultural and Forest Meteorology*, *256*, 501–515.
Merlin, O., Stefan, V. G., Amazirh, A., Chanzy, A., Ceschia, E., Er-Raki, S., et al. (2016). Modeling soil evaporation efficiency in a range of soil and atmospheric conditions using a meta-analysis approach. *Water Resources Research*, *52*, 3663–3684. https://doi.org/10.1002/2015WR018233
Merz, S., Pohlmeier, A., Vanderborght, J., van Dusschoten, D., & Vereecken, H. (2015). Transition of stage I to stage II evaporation regime in the topmost soil: High-resolution NMR imaging, profiling and numerical simulation. *Microporous and Mesoporous Materials*, *205*, 3–6.
Michel, D., Jiménez, C., Miralles, D. G., Jung, M., Hirschi, M., Ershadi, A., et al. (2016). The WACMOS-ET project–Part 1: Tower-scale evaluation of four remote-sensing-based evapotranspiration algorithms. *Hydrology and Earth System Sciences*, *20*(2), 803–822.
Millington, R. J., & Quirk, J. P. (1961). Permeability of porous solids. *Transactions of the Faraday Society*, *57*, 1200–1207.
Milly, P. C. D. (1984a). A linear analysis of thermal effects on evaporation from soil. *Water Resources Research*, *20*(8), 1075–1085.
Milly, P. C. D. (1984b). A simulation analysis of thermal effects on evaporation from soil. *Water Resources Research*, *20*(8), 1087–1098.
Miralles, D. G., Holmes, T. R. H., De Jeu, R. A. M., Gash, J. H., Meesters, A. G. C. A., & Dolman, A. J. (2011). Global land-surface evaporation estimated from satellite-based observations. *Hydrology and Earth System Sciences*, *15*(2), 453.
Mualem, Y. (1976). A new model for predicting the hydraulic conductivity of unsaturated porous media. *Water Resources Research*, *12*(3), 513–522.
Noilhan, J., & Planton, S. (1989). A simple parameterization of land surface processes for meteorological models. *Monthly Weather Review*, *117*(3), 536–549.
Novick, K. A., Stoy, P. C., Katul, G. G., Ellsworth, D. S., Siqueira, M. B. S., Juang, J., & Oren, R. (2004). Carbon dioxide and water vapor exchange in a warm temperate grassland. *Oecologia*, *138*(2), 259–274.
Oki, T., & Kanae, S. (2006). Global hydrological cycles and world water resources. *Science*, *313*(5790), 1068–1072.
Or, D., & Lehmann, P. (2019). Surface evaporative capacitance–How soil type and rainfall characteristics affect global scale surface evaporation. *Water Resources Research*, *55*, 519–539. https://doi.org/10.1029/2018WR024050
Or, D., Lehmann, P., Shahraeeni, E., & Shokri, N. (2013). Advances in soil evaporation physics—A review. *Vadose Zone Journal*, *12*(4).
Papale, D., Reichstein, M., Aubinet, M., Canfora, E., Bernhofer, C., Kutsch, W., et al. (2006). Towards a standardized processing of Net Ecosystem Exchange measured with eddy covariance technique: Algorithms and uncertainty estimation. *Biogeosciences*, *3*(4), 571–583. https://doi.org/10.5194/bg-3-571-2006
Penman, H. L. (1948). Natural evaporation from open water, bare soil and grass. *Proceedings of the Royal Society of London. Series A*, *193*(1032), 120–145.
Peters, A. (2013). Simple consistent models for water retention and hydraulic conductivity in the complete moisture range. *Water Resources Research*, *49*, 6765–6780. https://doi.org/10.1002/wrcr.20548
Philip, J. R., & De Vries, D. A. (1957). Moisture movement in porous materials under temperature gradients. *Eos, Transactions American Geophysical Union*, *38*(2), 222–232.
Priestley, C. H. B., & Taylor, R. J. (1972). On the assessment of surface heat flux and evaporation using large-scale parameters. *Monthly Weather Review*, *100*(2), 81–92.
Saito, H., Šimůnek, J., & Mohanty, B. P. (2006). Numerical analysis of coupled water, vapor, and heat transport in the vadose zone. *Vadose Zone Journal*, *5*(2), 784–800.
Saravanapavan, T., & Salvucci, G. D. (2000). Analysis of rate-limiting processes in soil evaporation with implications for soil resistance models. *Advances in Water Resources*, *23*(5), 493–502.
Scherer, G. W. (1990). Theory of drying. *Journal of the American Ceramic Society*, *73*(1), 3–14.
Schlesinger, W. H., & Jasechko, S. (2014). Transpiration in the global water cycle. *Agricultural and Forest Meteorology*, *189*, 115–117.
Schneider, M., & Goss, K.-U. (2012). Prediction of the water sorption isotherm in air dry soils. *Geoderma*, *170*, 64–69. https://doi.org/10.1016/j.geoderma.2011.10.008
Seneviratne, S. I., Corti, T., Davin, E. L., Hirschi, M., Jaeger, E. B., Lehner, I., et al. (2010). Investigating soil moisture–climate interactions in a changing climate: A review. *Earth-Science Reviews*, *99*(3-4), 125–161.
Shahraeeni, E., Lehmann, P., & Or, D. (2012). Coupling of evaporative fluxes from drying porous surfaces with air boundary layer: Characteristics of evaporation from discrete pores. *Water Resources Research*, *48*, W09525. https://doi.org/10.1029/2012WR011857
Shokri, N., Lehmann, P., & Or, D. (2009). Critical evaluation of enhancement factors for vapor transport through unsaturated porous media. *Water Resources Research*, *45*, W10433. https://doi.org/10.1029/2009WR007769
Shokri, N., Lehmann, P., Vontobel, P., & Or, D. (2008). Drying front and water content dynamics during evaporation from sand delineated by neutron radiography. *Water Resources Research*, *44*, W06418. https://doi.org/10.1029/2007WR006385
Shokri, N., & Or, D. (2011). What determines drying rates at the onset of diffusion controlled stage-2 evaporation from porous media? *Water Resources Research*, *47*, W09513. https://doi.org/10.1029/2010WR010284
Sutanto, S. J., Wenninger, J., Coenders-Gerrits, A. M. J., & Uhlenbrook, S. (2012). Partitioning of evaporation into transpiration, soil evaporation and interception: A comparison between isotope measurements and a HYDRUS-1D model. *Hydrology and Earth System Sciences*, *16*(8), 2605–2616.
Tokunaga, T. K. (2009). Hydraulic properties of adsorbed water films in unsaturated porous media. *Water Resources Research*, *45*, W06415. https://doi.org/10.1029/2009WR007734
Trenberth, K. E., Fasullo, J. T., & Kiehl, J. (2009). Earth's global energy budget. *Bulletin of the American Meteorological Society*, *90*(3), 311–324.
Tuller, M., & Or, D. (2001). Hydraulic conductivity of variably saturated porous media: Film and corner flow in angular pore space. *Water Resources Research*, *37*(5), 1257–1276. https://doi.org/10.1029/2000WR900328

Tuller, M., & Or, D. (2005). Water films and scaling of soil characteristic curves at low water contents. *Water Resources Research*, *41*, W09403. https://doi.org/10.1029/2005WR004142

Tuller, M., Or, D., & Dudley, L. M. (1999). Adsorption and capillary condensation in porous media: Liquid retention and interfacial configurations in angular pores. *Water Resources Research*, *35*(7), 1949–1964.

van Genuchten, M. T. (1980). A closed-form equation for predicting the hydraulic conductivity of unsaturated soils. *Soil Science Society of America Journal*, *44*, 892–898. https://doi.org/10.2136/sssaj1980.03615995004400050002x

Wallace, J. S., Allen, S. J., Gash, J. H. C., Holwill, C. J., & Lloyd, C. R. (1993). *Components of the energy and water balance at the HAPEX-Sahel southern super-site* (pp. 365–365). Iahs Publication.

Wang, K., & Dickinson, R. E. (2012). A review of global terrestrial evapotranspiration: Observation, modeling, climatology, and climatic variability. *Reviews of Geophysics*, *50*, RG2005. https://doi.org/10.1029/2011RG000373

Wang, Y., Jin, M., & Deng, Z. (2018). Alternative model for predicting soil hydraulic conductivity over the complete moisture range. *Water Resources Research*, *54*, 6860–6876. https://doi.org/10.1029/2018WR023037

Wang, Y., Ma, J., & Guan, H. (2016). A mathematically continuous model for describing the hydraulic properties of unsaturated porous media over the entire range of matric suctions. *Journal of Hydrology*, *541*, 873–888.

Wang, Y., Ma, J., Guan, H., & Zhu, G. (2017). Determination of the saturated film conductivity to improve the EMFX model in describing the soil hydraulic properties over the entire moisture range. *Journal of Hydrology*, *549*, 38–49.

Wang, Y., Ma, J., Zhang, Y., Zhao, M., & Edmunds, W. M. (2013). A new theoretical model accounting for film flow in unsaturated porous media. *Water Resources Research*, *49*, 5021–5028. https://doi.org/10.1002/wrcr.20390

Wilson, G. W. (1990). Soil evaporative fluxes for geotechnical engineering problems (Doctoral dissertation, University of Saskatchewan).

Wu, C., Chen, J. M., Pumpanen, J., Cescatti, A., Marcolla, B., Blanken, P. D., et al. (2012). An underestimated role of precipitation frequency in regulating summer soil moisture. *Environmental Research Letters*, *7*(2).

Yiotis, A. G., Boudouvis, A. G., Stubos, A. K., Tsimpanogiannis, I. N., & Yortsos, A. Y. (2003). Effect of liquid films on the isothermal drying of porous media. *Physical Review E*, *68*(3).

Yiotis, A. G., Salin, D., Tajer, E. S., & Yortsos, Y. C. (2012). Drying in porous media with gravity-stabilized fronts: Experimental results. *Physical Review E*, *86*(2).

Yiotis, A. G., Tsimpanogiannis, I. N., Stubos, A. K., & Yortsos, Y. C. (2007). Coupling between external and internal mass transfer during drying of a porous medium. *Water Resources Research*, *43*, W06403. https://doi.org/10.1029/2006WR005558

Zhang, C., Li, L., & Lockington, D. (2015). A physically based surface resistance model for evaporation from bare soils. *Water Resources Research*, *51*, 1084–1111. https://doi.org/10.1002/2014WR015490